Available online at www.sciencedirect.com
SCIENCE DIRECT®
International Journal of Plasticity 22 (2006) 1549–1568
INTERNATIONAL JOURNAL OF Plasticity
www.elsevier.com/locate/ijplas

Compressive properties of epoxidized soybean oil/clay nanocomposites

Bo Song [a], Weinong Chen [b,*], Zengshe Liu [c], Sevim Erhan [c]

[a] *School of Aeronautics and Astronautics, Purdue University, West Lafayette, IN 47907, United States*
[b] *Schools of Aeronautics and Astronautics and Materials Engineering, Purdue University, West Lafayette, IN 47907, United States*
[c] *NCAUR, ARS, USDA, 1815 N. University Street, Peoria, IL 61604, United States*

Received 24 February 2005
Available online 26 January 2006

Abstract

High- and low strain-rate compression experiments were conducted on epoxidized soybean oil (ESO)/clay nanocomposites with nanoclay weights of 0%, 5%, and 8%. A pulse-shaped split Hopkinson pressure bar (SHPB) was employed to conduct high strain-rate experiments. The pulse shaping technique ensures nearly constant-strain-rate deformation under dynamically equilibrated stresses in specimens such that accurate stress–strain curves at various high rates were obtained. A MTS 810 hydraulically driven materials testing system was used to obtain low strain-rate stress–strain curves. Strain-rate and nanoclay weight effects on the compressive properties of the nanocomposites were experimentally determined. A phenomenological strain-rate-dependent material model was presented to describe the stress–strain response. The model agrees well with the experimental data at both large and small strains as well as high and low strain rates.

Keywords: Compressive properties; Nanocomposite; Split Hopkinson pressure bar (SHPB); Strain-rate; Material model

1. Introduction

During the recent years, increasing attention has been paid to polymers obtained from renewable resources. This interest is justified by the environmental advantage of these

* Corresponding author. Tel.: +1 765 494 1788.
E-mail address: wchen@purdue.edu (W. Chen).

0749-6419/$ - see front matter
doi:10.1016/j.ijplas.2005.10.004

materials, which are neutral in carbon dioxide cycle and often biodegradable. These polymers may also constitute a new outlet for vegetable products. Among products from agricultural resources, natural oils may constitute raw materials useful in polymer synthesis. For example, United States agriculture produces over 12 billion pounds of soybean oil annually, and frequently carry-over exceeds one billion pounds. Thus, developing new materials from soybean oil for industrial application has become highly desirable. These new materials can open new market for this important crop.

Soybean oil is a double bond containing triglyceride. These double bonds may also be converted into the more reactive oxirane moiety by reaction with peracids or peroxides. In the past, epoxidized soybean oil (ESO) is mainly used as platicizer for polyvinyl chloride, chlorinated rubber and polyvinyl emulsions to improve stability and flexibility. The preparation of structurally strong soy-based composites is attractive from both commercial and environmental perspectives. Soy composites can be reinforced with glass, carbon or natural fibers. Proper combination of natural clay and soybean oil can form nanocomposites that have unique properties and applications.

Since the Toyota group developed the nylon 6-clay hybrid (Okada et al., 1989; Kojima et al., 1993a,b,c,d, 1994, 1995; Usuki et al., 1995), the interest in nanocomposites has been inspired by the fact that nanoscale materials often exhibited dramatically different properties, such as gas permeability (Kojima et al., 1993e), water absorption (Kojima et al., 1994c; Drozdov et al., 2003; Kim et al., 2003), chemical (Okada and Usuki, 1995), thermal (Hao et al., 2002; Kim et al., 2003; Lee et al., 2003), and mechanical properties (Okada et al., 1989; Kojima et al., 1993b; Lan and Pinnavaia, 1994; Usuki et al., 1995; LeBaron et al., 1999; Tyan et al., 2000; Nam et al., 2001; Sur et al., 2001; Tien and Wei, 2001; Zerda and Lesser, 2001; Zhou et al., 2001; Abdalla et al., 2002; Ha and Thomas, 2002; Hao et al., 2002; Svoboda et al., 2002; Young and Mauritz, 2002; Chen et al., 2003; Drozdov et al., 2003; Kim et al., 2003; Lee et al., 2003; Liu et al., 2003; Uribe-Arocha et al., 2003; Zhang et al., 2003) from their bulk counterparts, which is earning them wide applications in automobile and transportation industries, construction and fire-safety engineering, and even military armors. One of the most promising composite systems would be organic polymers (i.e., nylon 6) and inorganic clay minerals consisting of silicate layers. As an inexpensive natural mineral, clay has been used as filler for rubbers and plastics for many years. However, its poor reinforcing ability limits its usage only for conventional microcomposites. In order to improve the reinforcing ability of clay, chemical modifications with various chemistries have been recently developed to make the clay complexes compatible with organic monomers and polymers.

While more and more nanocomposites are developed, the synthesis, morphology and structure of nanocomposites have been well reviewed by Okada and Usuki (1995), Giannelis (1996), LeBaron et al. (1999), Sur et al. (2001), and Hamley (2003) in recent years. These nanocomposites are recognized to reduce shrinkage and residual stress, to alter electrical, electronic and optical properties, to improve thermal endurance, flame resistance, abrasion resistance, and barrier properties, as well as to efficiently reinforce mechanical properties (Hamley, 2003). In addition, many potential benefits such as fire resistance, electrostatic dissipation (ESD), and electromagnetic interference (EMI) are being developed (Hamley, 2003). Among these properties, the research on mechanical properties of nanocomposites is attracting more and more researchers' attention.

One of the motivations for optimizing nanocomposites is to improve their mechanical properties. Besides low strain-rate compression and fracture toughness tests by LeBaron

et al. (1999) and Zerda and Lesser (2001), low strain-rate tension tests have been performed on nanocomposites to understand their mechanical properties and to examine the effects of nanoclay contents on the mechanical properties, i.e., modulus of elasticity and yield strength, of the nanocomposites. It has been concluded that the modulus of elasticity increases with the nanoclay weight (Kojima et al., 1993a; Lan and Pinnavaia, 1994; LeBaron et al., 1999; Tyan et al., 2000; Zerda and Lesser, 2001; Zhou et al., 2001; Ha and Thomas, 2002; Hao et al., 2002; Svoboda et al., 2002; Chen et al., 2003; Kim et al., 2003; Lee et al., 2003; Liu et al., 2003) since the effects of nanoclay in a nanocomposite (nylon 6/clay hybrid) on the modulus of elasticity were studied (Okada et al., 1989; Kojima et al., 1993b; Usuki et al., 1995). However, the effects of nanoclay on tensile strength are much more complicated. The Toyota group found that the existence of nanoclay significantly increased the tensile strength of nylon 6/clay hybrid (Okada et al., 1989; Kojima et al., 1993b; Usuki et al., 1995). Similar conclusions have been obtained for the other nanocomposites including epoxy/clay presented by Lan and Pinnavaia (1994), clay-polyimide by Tyan et al. (2000), polyurethane/silicate by Tien and Wei (2001), roll-cast layered-silicate/lamellar styrene–isoprene–styrene (SIS) triblock copolymer nanocomposite by Ha and Thomas (2002), Nafion/silicate by Young and Mauritz (2002), polyurethane/clay nanocomposite by Kim et al. (2003), nanoclay-filled polypropylene by Chen et al. (2003), and nylon 11/organoclay nanocomposite by Liu et al. (2003). By contrast, Hao et al. (2002) found that, with the increasing clay weight, the yield strength varied little and the fracture strength decreased. Moreover, it has been observed that, as compared to the bulk materials without clay, the low strain-rate tensile strengths of the nanocomposites decreased due to the existence of clay (Zhou et al., 2001; Hao et al., 2002; Svoboda et al., 2002; Lee et al., 2003). By adding a nanoclay phase to EPDM rubber, Ahmadi et al. (2005) found that the mechanical properties were enhanced initially with increasing clay load, but trend reversed when excessive clay was added. They concluded that inevitable aggregation of the clay layers at high clay volume caused the damaging effects. A similar trend was documented by Kinlock and Taylor (2003) on the fracture toughness of nano mica composites. The research by Wanjale and Jog (2003) attempted to improve the compatibility of the nano phase with the matrix material. Hwu et al. (2002) and Kornmann et al. (2002) conducted similar researches on different material systems. Thus, conflicting conclusions on mechanical improvement of nanoclay particles in the nanocomposites exist in current research results.

Even though the nanocomposites have been proposed to be used in the applications subjected to impact loading, high strain-rate mechanical properties of nanocomposites have been less documented except the dynamic viscoelastic measurements (Tyan et al., 2000; Nam et al., 2001; Abdalla et al., 2002; Liu et al., 2003; Uribe-Arocha et al., 2003), Charpy and Izod impact tests (Okada et al., 1989; Kojima et al., 1993b; Svoboda et al., 2002). These dynamic measurements did not provide families of stress–strain curves with a function of strain-rate, which are necessary to develop strain-rate-dependent material models for the purpose of numerical simulations and design optimizations in impact applications. As an efficient dynamic experimental technique, split Hopkinson pressure bar (SHPB) has been widely employed to obtain stress–strain curves of engineering materials in the strain-rate range of 10^2–10^3/s (Kolsky, 1949). When the split Hopkinson bar is used to test soft materials such as polymers, the applicability needs to be carefully examined because it is difficult to ensure that the specimen deforms at a nearly constant strain-rate under dynamically equilibrated stresses in a conventional SHPB experiment that is

required to obtain valid stress–strain data (Chen et al., 2002). Therefore, modifications on the SHPB technique for testing soft material are necessary to obtain valid and accurate high strain-rate results for soft materials at high strain rates (Chen et al., 2002).

Due to scarcity of experimental data, strain-rate-dependent material models for nanocomposites have been less developed and documented. Strain-energy functions have been commonly used to describe the stress–strain behavior of hyperelastic solids under low strain-rate loading conditions (Ward, 1983; Chen and Wang, 1997; Ogden and Roxburgh, 1999). This strain-energy function is efficient to describe large-deformation response although the strain-rate effects are not accounted for. In order to describe the strain-rate-dependent response at large strains, additional strain-rate-sensitivity terms are necessary. A strain-rate-dependent material model based on relaxation function for viscoelastic solids has also been developed (Wang et al., 1995). This model is ideal to describe strain-rate-dependent viscoelastic response of materials at small strains. To properly describe the rate-dependent non-linear stress–strain behavior over the entire strain span, it is necessary to combine the strain-energy function for hyperelastic solids and the relaxation function for viscoelastic solids. Such a model has been developed and applied to describe the strain-rate-dependent stress–strain behavior of rubber materials (Song et al., 2004).

In this study, we employed a modified SHPB to determine high strain-rate compressive stress–strain curves of ESO/clay nanocomposites, which contain nanoclay weights of 0%, 5%, and 8%, respectively. Low strain-rate compressive stress–strain curves were also obtained to extensively examine the strain-rate effects in a wide strain-rate range. The effects of nanoclay weight on the compressive properties were also investigated. The experimental data were then phenomenologically modeled with a combination of a strain-rate-dependent strain-energy function for hyperelastic solids and a relaxation function for viscoelastic solids.

2. Experiments

2.1. Materials and specimens

In this research, ESO (oxirane contains as 7.0%) was obtained from Elf Atochem Inc. (Philadelphia, PA). Triethylenetetramine (TETA), 60% tech was provided by Aldrich Chemical Inc. (Milwaukee, WI). Closite 30B (montmorillonite modified with alkyl quaternary ammonium montmorillonite), used as filler, was obtained from Southern Clay Products, Inc.

The ESO was mixed with Cloisite 30B particles at 60 °C for 2 h using a mechanical stirrer. The mixture was sonicated at 60 °C for 2 h, followed by degassing at this temperature for a half of hour. Designated amount of curing agent, TETA, was then added to the mixture at stoichiometric ratio at room temperature and the pre-mix at room temperature. The mixture was stirred for 15 min, followed by degassing at 60 °C for 15 min. Then the mixture was poured into a container made from transparency film, and cured in an oven at 60 °C for 16 h, then at 120 °C for 48 h. The components and their amounts in the mixtures are tabulated in Table 1. Powder XRD analysis was performed at room temperature using a Philips 1830 diffractometer operated at 40 kV, 30 mA with graphite-filtered Cu Kα ($\lambda = 0.154$ nm) radiation and a θ compensating slit. Data were acquired in $2\theta = 0.05°$, 4 s steps. The scanning range is from 2.5° to 10°.

Table 1
Strain-rate and nanoclay-weight effects on stresses at certain strains

	ESO:H = 1:1.37					
Components	ESO/clay-0		ESO/clay-5		ESO/clay-8	
Nanoclay weight	0		5%		8%	
Strain	Strain rate (s^{-1})	Stress (MPa)	Strain rate (s^{-1})	Stress (MPa)	Strain rate (s^{-1})	Stress (MPa)
5%	10^{-3}	0.12	10^{-3}	0.15	10^{-3}	0.16
	10^{-2}	0.19	10^{-2}	0.23	10^{-2}	0.26
	10^{-1}	0.37	10^{-1}	0.53	10^{-1}	0.60
	15	15.62	15	16.60	15	10.07
	550	44.96	430	41.72	700	26.24
	2450	58.13	1930	48.22	2540	26.01
10%	10^{-3}	0.25	10^{-3}	0.30	10^{-3}	0.33
	10^{-2}	0.34	10^{-2}	0.43	10^{-2}	0.48
	10^{-1}	0.63	10^{-1}	0.88	10^{-1}	1.02
	15	22.63	15	24.76	15	18.65
	550	/	550	52.95	550	37.52
	2450	74.36	1930	68.93	2540	40.22
40%	10^{-3}	1.72	10^{-3}	2.13	10^{-3}	2.42
	10^{-2}	1.94	10^{-2}	2.62	10^{-2}	3.22
	10^{-1}	3.05	10^{-1}	4.66	10^{-1}	5.51
	15	39.83	15	43.35	15	37.72
	550	/	550	/	550	/
	2450	112.28	1930	119.02	2540	79.65

The XRD patterns of the nanocomposites and the particle are shown in Fig. 1, indicating a sharp peak at 4.5° for nanoclay. However, no peaks were detected using XRD for the composites with Cloisite 30B 5.0, and 8.0 wt%. Although it is common practice to classify a nanocomposite as fully exfoliated from the absence of (0 0 1) reflection, it is difficult to reach a definitive conclusion about the defined structure from the XRD alone. Thus transition electron microscopy (TEM) investigations were performed. The TEM specimens were cut from nanocomposites blocks using an ultramicotome (Sovall MT-2

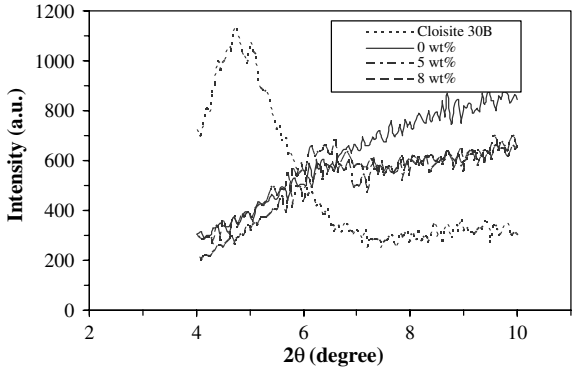

Fig. 1. X-ray diffraction patterns of the nanocomposites.

Ultramicrotome) equipped with a diamond knife. The TEM micrographs were taken with a Hitachi HF 2000 at an acceleration voltage of 200 kV. Fig. 2 shows TEM micrographs of ESO/clay nanocomposites containing 5.0, and 8.0 wt% content, respectively. TEM micrograph shows that there was no aggregation of organic particles. This suggests that the organic clay is well dispersed in ESO matrix. Layer spacing of the clay in the nanocomposites increased, compared to the organo-clay galleries about 2 nm. There was a distribution in basal spacings. A wide distribution in basal spacings may cause the absence of (0 0 1) reflection. Under this condition, it is clear that an intercalated structure of the composites was developed. However, the orientation of the nanolayers were found not well aligned in the materials.

The specimens for low strain-rate mechanical experiments were cut from sheet materials into cylinders with a diameter of ~8.0 mm and a thickness of ~6.0 mm. Those for high strain-rate experiments were cylinders with the same diameter but a smaller thickness of ~2.8 mm, because thinner specimens are necessary to achieve early dynamic stress equilibrium in the dynamic SHPB experiments for soft materials (Song and Chen, 2004).

2.2. High strain-rate experiments

As mentioned earlier, the conventional SHPB needs to be modified to obtain valid and accurate stress–strain behavior for soft materials. In this research, an aluminum SHPB, modified with pulse-shapers and quartz piezoelectric force transducers as described by Chen et al. (2002), was employed to investigate the high strain-rate compressive stress–strain responses of the three nanocomposites listed in Table 1. A schematic of the modified SHPB setup is shown in Fig. 3. Copper tubes were used as pulse shapers to ensure that the specimens deformed at nearly constant strain rates under dynamically equilibrated stresses. The profiles of loading pulses were modified to achieve various constant strain-rate levels through varying the diameter and length of the copper tube as well as the velocity of striker. Since it is very difficult to check dynamic stress equilibrium in a soft specimen by comparing the transmitted signal (1-wave) and the difference between the incident and reflected signals (2-wave) in a conventional SHPB test, quartz piezoelectric force transducers were used to directly monitor the process of dynamic stress equilibrium in the soft specimen during dynamic loading. The piezoelectric transducers used in this paper have a mechanical impedance of 1.438×10^8 kg/m^2 s, which is very close to 1.394×10^8 kg/m^2 s for the aluminum bar material. Furthermore, the force transducers are very thin (0.25 mm), which facilitate almost immediate stress equilibrium across the transducer. Therefore, the effects of introducing such piezoelectric transducers on the stress wave propagation are considered negligible. The signals from the quartz piezoelectric force transducers were recorded with a digital oscilloscope (Tektronix TDS 420A) through Kistler 5100 charge amplifiers. The digital oscilloscope was also utilized to record the signals from the strain gages (Vishay Micro-Measurements, WK-13-125BZ-10C) on the incident bar and the transmission bar through ADA400A differential pre-amplifiers.

A typical set of incident, reflected, and transmitted signals from such a pulse-shaped SHPB experiment on ESO/clay-8 at a strain-rate of 2540/s are shown in Fig. 4. In Fig. 4, the shape of incident pulse was modified through employing a copper tube as the pulse shaper to generate a nearly flat plateau in the reflected signal, indicating a nearly constant strain-rate if dynamic stress equilibrium in specimen is achieved. In addition, the pulse shaper generated an incident pulse without the high-frequency components com-

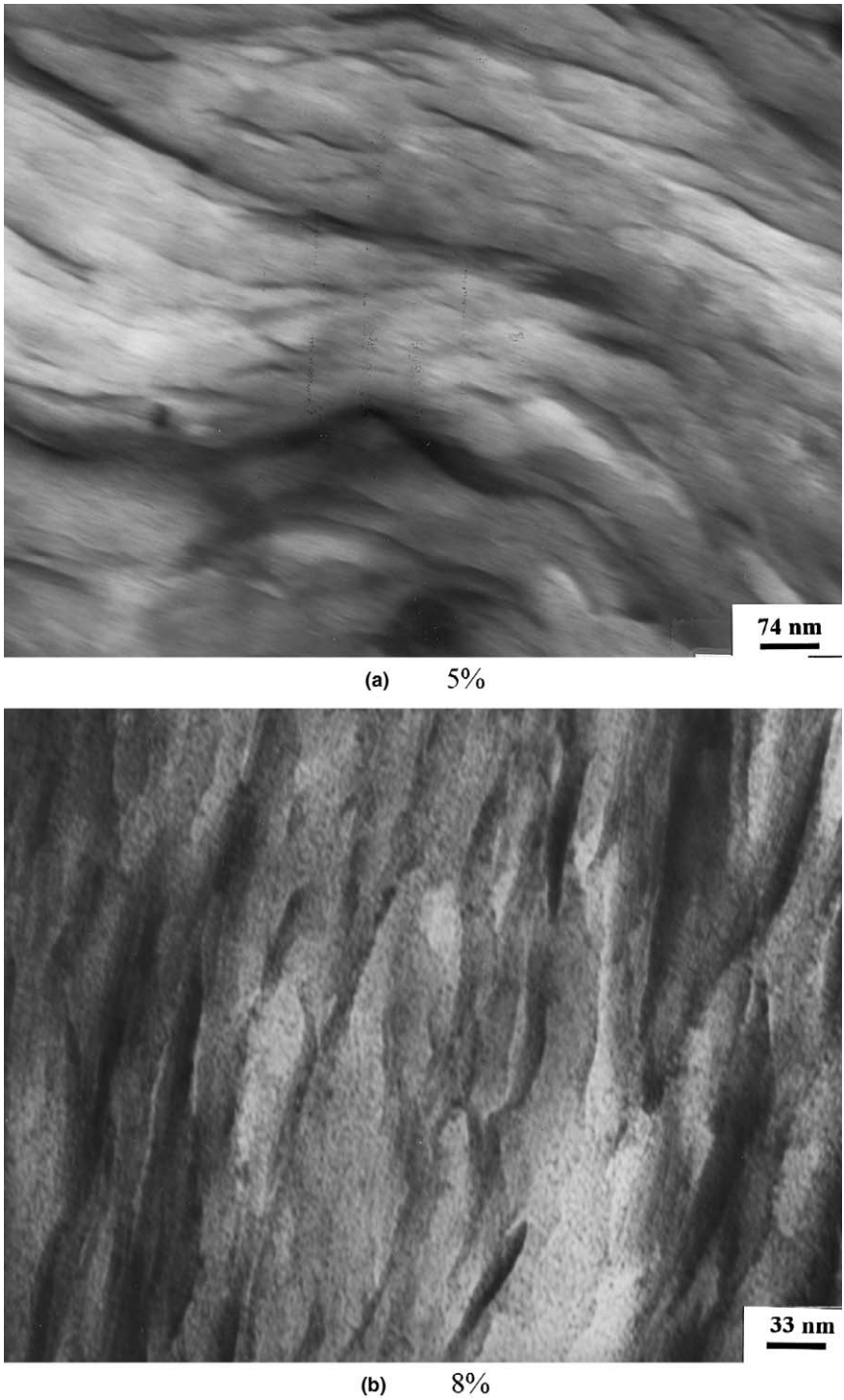

Fig. 2. Microstructures of the nanocomposites.

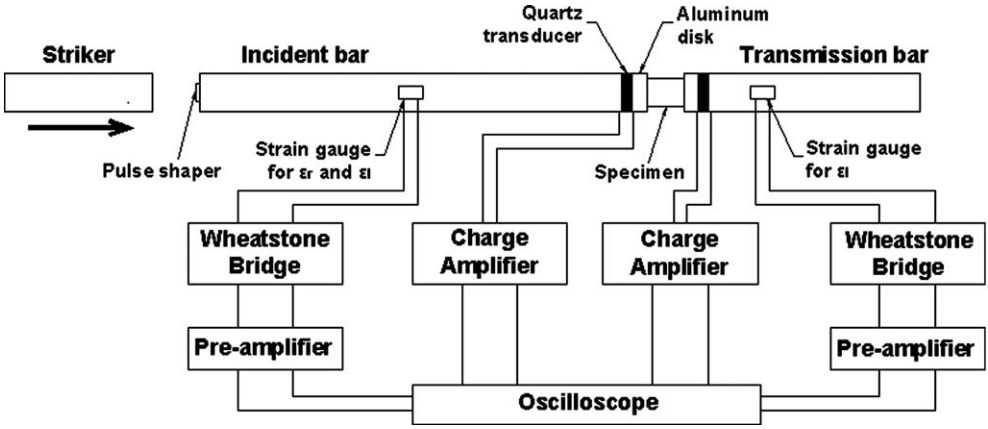

Fig. 3. A schematic of the modified SHPB setup.

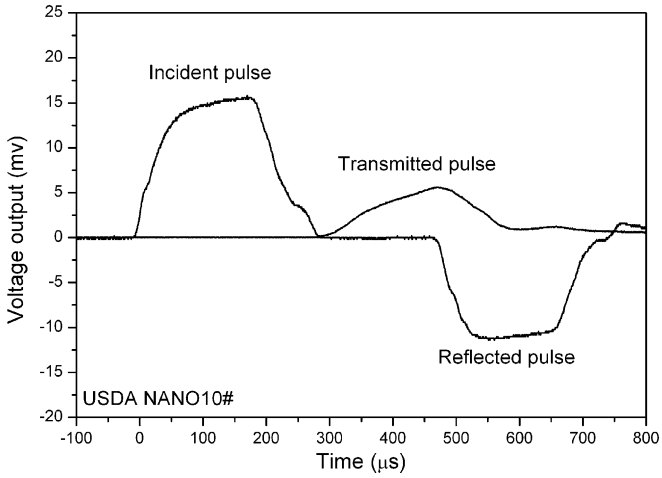

Fig. 4. A typical set of incident, reflected, and transmitted signals in an SHPB experiment on ESO/clay-8.

monly seen in a conventional SHPB. Therefore, the pulse is nearly dispersion free and further dispersion correction becomes unnecessary. The process of dynamic equilibrium may be monitored through relative error (Ravichandran and Subhash, 1994)

$$R(t) = \left|\frac{\Delta\sigma(t)}{\sigma_{\text{avg}}(t)}\right| = 2\left|\frac{F_1 - F_2}{F_1 + F_2}\right| \tag{1}$$

where $\Delta\sigma$ and σ_{avg} are the difference and averaged values between the stresses at both ends of the specimen, respectively; F_1 and F_2 are axial forces at the front-end (facing incident bar) and back-end (facing transmission bar) of the specimen, respectively. Although this analysis only applies to linearly elastic materials, the error indicator $R(t)$ is a generic

description of load imbalance along a certain direction, which is material independent. Here we borrow this relative error indicator to evaluate the dynamic stress equilibrium process in specimen. The $R(t)$ is shown in Fig. 5, the result of which indicates that dynamic force equilibrium was achieved at ~50 μs after the front-end was initially loaded. Fig. 6 shows the engineering stress–strain curve and the strain-rate history at the strain-rate of 2540/s. The fact of a nearly constant strain-rate beyond 5% strain where the stress equilibrium has been achieved (Fig. 5) indicates that the stress–strain curve in this figure is reliable and accurate to describe the dynamic compressive response of the nanocomposite at this strain-rate.

Following the same procedure, high strain-rate SHPB experiments were conducted on ESO/clay-0 specimens at strain rates of 550/s and 2450/s, ESO/clay-5 specimens at strain rates of 430/s and 1930/s, as well as ESO/clay-8 specimens at strain rates of 700/s and 2540/s. Under the same loading conditions including strain-rate, repeated experiments were performed and the results were found to be repeatable. The validity check was performed on each experiment to ensure the reliability and accuracy of the resultant stress–strain curves.

2.3. Low strain-rate experiments

To investigate the compressive behavior of these materials over a wide strain-rate range, low strain-rate compressive experiments were performed with a standard MTS 810 hydraulically driven materials testing system. Through the control of hydraulic actuator moving velocity in displacement control mode, low strain-rate stress–strain curves were obtained at five strain rates (0.001/s, 0.01/s, 0.1/s, 1.0/s, and 15/s) for each of the three materials. Since the high strain rates achieved in the SHPB experiments began at 10^2/s, we obtained stress–strain data in every order of magnitude in strain rates from 10^{-3} to 10^3/s. Similar to high strain-rate experiments, more than two experiments at each low strain-rate for each material were performed, the results of which were repeatable.

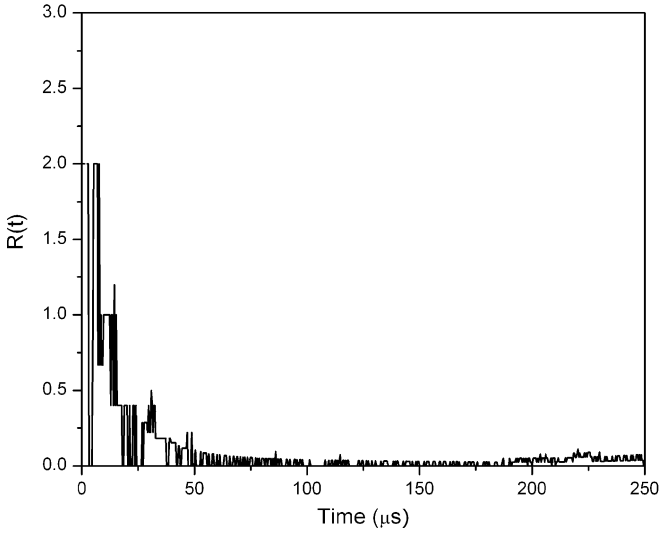

Fig. 5. Dynamic stress equilibrium process in an ESO/clay-8 specimen.

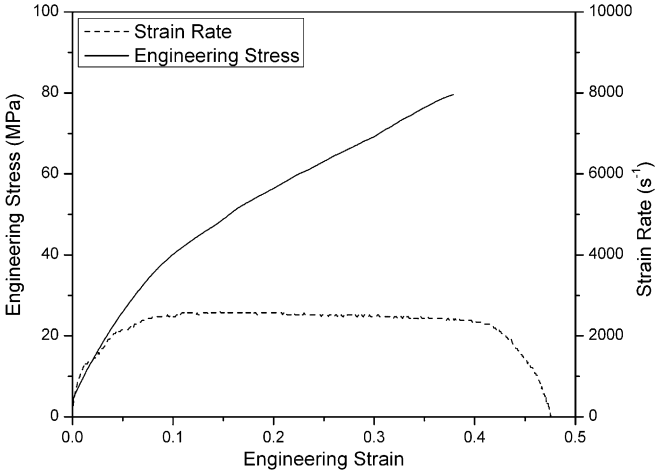

Fig. 6. Engineering stress–strain curve and strain-rate history of the ESO/clay-8 at the strain-rate of 2540/s.

2.4. Experimental results

The dynamic and quasi-static compressive stress–strain curves at various strain rates for the three materials (ESO/clay-0, ESO/clay-5 and ESO/clay-8) are shown in Fig. 7a–c, respectively.

The shapes of the stress–strain curves at the strain rates over 1.0/s are different from those of the stress–strain curves obtained at strain rates below 1.0/s, as shown in Fig. 7a–c. There is an initial nearly linear behavior followed by a transitional non-linear response and then a strain-hardening behavior in the stress–strain curves at strain rates over 1.0/s. By contrast, the initial linear behavior disappears in the stress–strain curves at lower strain rates, as shown in Fig. 7a–c. The non-linear strain-hardening behavior dominated the stress–strain response at the lower strain rates: the tangential modulus increases with increasing strains. Therefore, the strain-rate affects not only the strength but also the shape of stress–strain curve for the nanocomposites. The fact that all the specimens recovered with no or little residual strain after being compressed up to 40% of the maximum strain under dynamic loading conditions or 75% under low strain-rate loading conditions demonstrates the capabilities of the materials subjected to large deformation.

Table 1 lists the engineering stresses at the engineering strains of 5%, 10%, and 40% at various strain rates for the three materials. The data at the strains of 10% and 40% in Table 1 are illustrated in Figs. 8 and 9, respectively. Figs. 8 and 9 clearly indicate significant strain-rate effects for the three materials: the stresses at the certain strains increased with the increasing strain rates. It is noted that, for the material with nanoclay of 8% weight (ESO/clay-8), the stress at the strain of 5% at the strain-rate of 2540/s is a little lower than that at the strain-rate of 700/s (Table 1). The disappearance of strain-rate hardening at this nanoclay weight may be induced by interface damage between the nanoclay and the ESO material. The ESO/clay-0 material is included here as a reference. In the range of low strain rates, the stress for ESO/clay-0 at a strain of 5% increased from 0.12 MPa at the strain-rate of 0.001/s to 0.37 MPa at the strain-rate of 0.1/s. When the strain-rate is in high strain-rate range, the stress at the strain of 5% increases to 44.96 MPa at the strain-rate of 550/s and 58.13 MPa

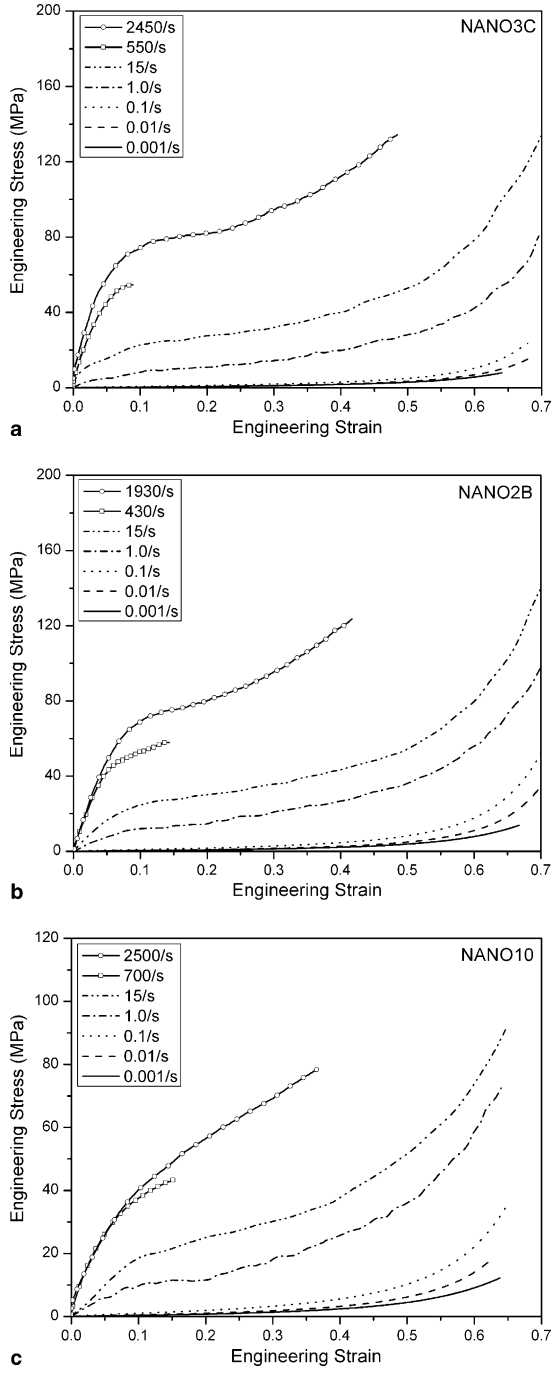

Fig. 7. Dynamic and quasi-static compressive stress–strain curves at various strain rates. (a) ESO/clay-0; (b) ESO/clay-5; (c) ESO/clay-8.

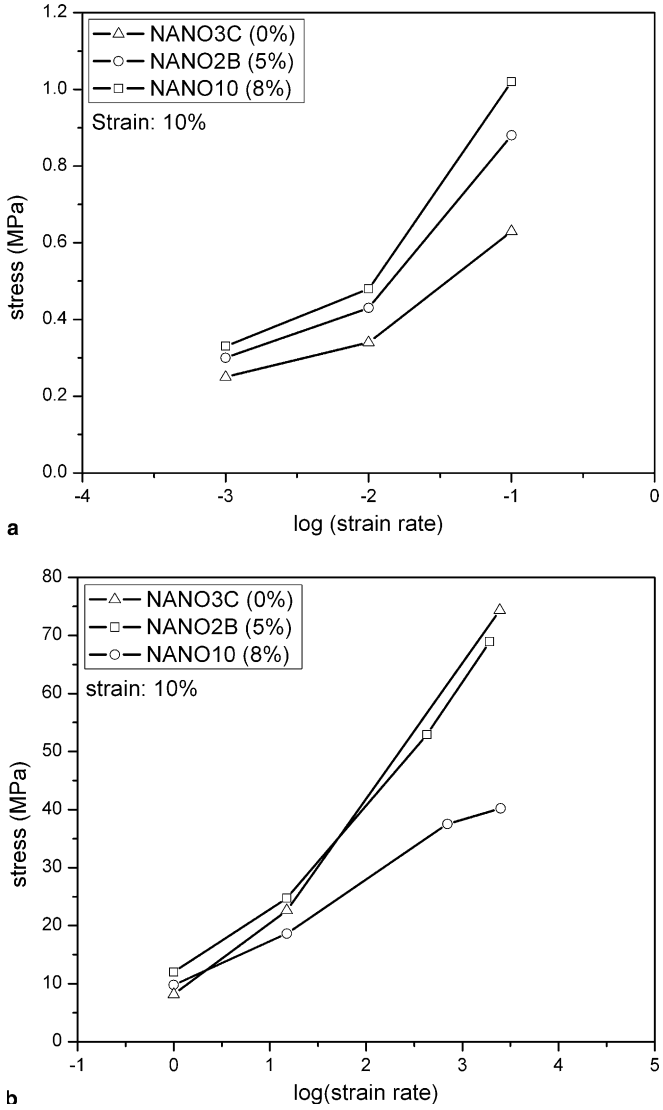

Fig. 8. Stresses at the strain of 5% for the nanocomposites at various strain rates. (a) $\dot{\varepsilon} \leqslant 0.1/\mathrm{s}$; (b) $\dot{\varepsilon} \geqslant 1.0/\mathrm{s}$.

at the strain-rate of 2450/s, which are much higher than the corresponding values obtained at strain rates a few orders of magnitude lower.

Compared to the significant strain-rate effects of the three materials, the nanoclay weight effects at similar strain rates were observed to be more complicated. In the range of strain rates below 1.0/s, the stress reinforced due to increasing nanoclay weight, as shown in Figs. 8a and 9a. For example, at the strain-rate of 0.01/s, the material without nanoclay (ESO/clay-0) exhibited the stress of 0.19 MPa at the strain of 5% and 1.94 MPa at the strain of 40%. The stress increased to 0.23 MPa at the strain of 5% and 2.62 MPa at the strain of 40% for the material with nanoclay of 5% weight (ESO/clay-5); whereas the

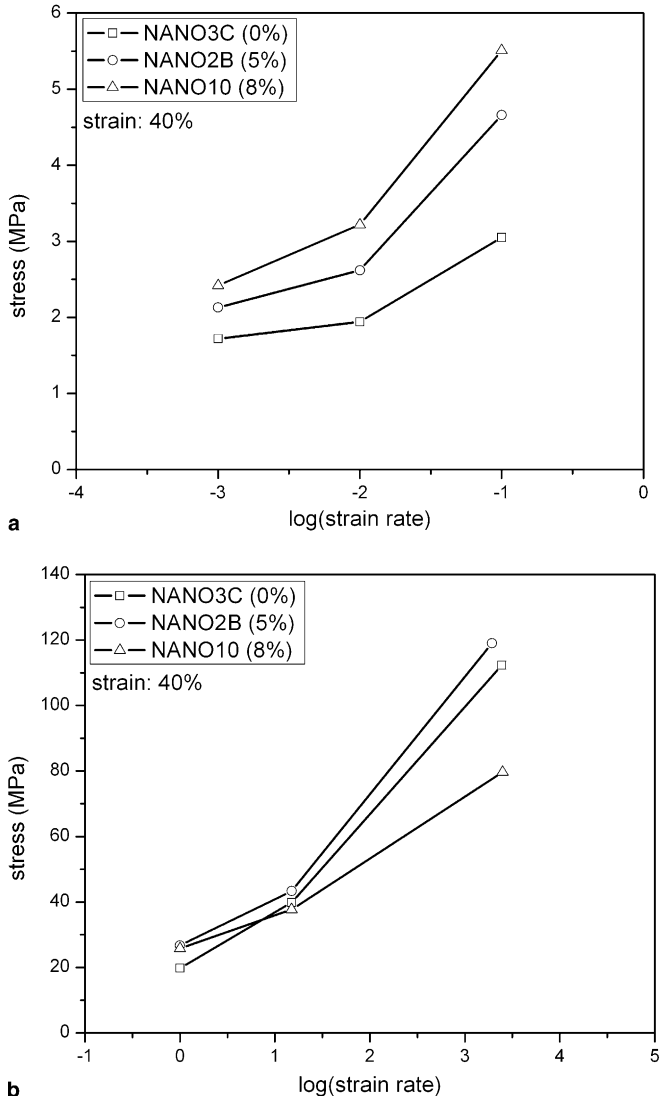

Fig. 9. Stresses at the strain of 40% for the nanocomposites at various strain rates. (a) 9; (b) $\dot{\varepsilon} \geqslant 1.0/\text{s}$.

stress further increased to 0.26 MPa at the strain of 5% and 3.22 MPa at the strain of 40% for the material with nanoclay of 8% weight (ESO/clay-8). The stress for the nanocomposites (ESO/clay-5 and ESO/clay-8) at the strain-rate of 1.0/s increased in comparison with the material without nanoclay (ESO/clay-0). However, the stress for ESO/clay-8 (8% weight nanoclay) is lower than that for ESO/clay-5 (5% weight nanoclay) at the strain-rate of 1.0/s. When the strain-rate increased to 15/s, the stress for ESO/clay-5 (5% weight nanoclay) increased whereas the stress for ESO/clay-8 (8% weight nanoclay) decreased as compared to ESO/clay-0 (0% weight nanoclay). In the range of high rates, the stresses at small strains for the materials with nanoclay are lower than those for the material

without nanoclay. The stress decreased more with the increasing nanoclay weight in the nanocomposites. At the large strains, the dynamic stress increased slightly when 5% weight nanoclay was added, and then decreased significantly for the material with 8% weight nanoclay. In details, ESO/clay-0 (0% weight nanoclay) had a stress of 58.13 MPa at the strain of 5% and the strain-rate of 2450/s; whereas ESO/clay-5 and ESO/clay-8 had stresses, at the strain of 5%, of 48.22 MPa and 26.01 MPa at similar strain rates. When the strain increased to ~40%, the stress increased to 112.28 MPa at the strain-rate of 2450/s for ESO/clay-0, whereas the corresponding stresses for ESO/clay-5 was 119.02 MPa, and ESO/clay-8 only 79.65 MPa at similar strain rates. At such high strain rates (10^3/s), the stress at the strain of 40% for the material with nanoclay of 8% weight dropped 30% as compared to the values for ESO/clay-0 and ESO/clay-5, indicating that the material containing too much nanoclay may not improve strength of material due to possible increasing interface damage in material, which needs further investigation for details. Inevitable aggregation of the clay layers at high clay volume has also been recognized as a possible mechanism for the damaging effects to the mechanical properties by high clay content (Ahmadi et al., 2005). To summarize the experimental results in a concise way that can be used for numerical simulations of structural responses, a phenomenological strain-rate-dependent material model is presented in the following session.

3. One-dimensional phenomenological strain-rate-dependent material model

As demonstrated by the experimental results, all three materials exhibited non-linear stress–strain responses with strain-rate sensitivity. Non-linear behavior is conventionally described by strain-energy functions, which has been used for hyperelastic solids. However, strong strain-rate sensitivity is a typical viscoelastic/viscoplastic response. Since the materials investigated in this research exhibited both non-linearity and strain-rate sensitivity, we combined a strain-energy functions and a viscoelastic framework to describe the strain-rate-dependent non-linear response of materials. A model based on a strain-energy function for hyperelastic solids and a relaxation function for viscoelastic solids has been developed and applied in modeling stress–strain behavior of rubber materials (Song et al., 2004). There are a number of polymer material models that describe the strain-rate- and temperature-dependent behaviors (e.g., Lion and Kardelky, 2004; Colak, 2005; Makradi et al., 2005; Khan et al., 2006). In this study, we utilized the form of the material model developed by Song et al. (2004) to describe the stress–strain behavior of the nanocomposites due to a similar application strain-rate range

$$\sigma_T = f_1(\dot{\varepsilon}) \cdot \left(1 - \varepsilon - \frac{1}{(1-\varepsilon)^2}\right) + f_2(\dot{\varepsilon}) \cdot \left(1 - e^{-\frac{\varepsilon}{\varepsilon_r}}\right) \tag{2}$$

where ε_r is a material constant; $f_1(\dot{\varepsilon})$ and $f_2(\dot{\varepsilon})$ are the terms to describe strain-rate effects at small and large strains, respectively. After curve-fitting, we found the following formulations can faithfully describe the strain-rate effects,

$$f_1(\dot{\varepsilon}) = A_1 \left(\frac{\dot{\varepsilon}}{\dot{\varepsilon}_0}\right)^{t_1} \tag{3}$$

$$f_2(\dot{\varepsilon}) = A_2 + A_3 \log \frac{\dot{\varepsilon}}{\dot{\varepsilon}_0} \tag{4}$$

Table 2
Material constants for the nanocomposites

		ESO/clay-0	ESO/clay-5	ESO/clay-8
ε_r		0.035		
$\dot{\varepsilon}_0$		0.001		
t_1		0.1265		0.1766
A_1		−0.3307	−0.5735	−0.5634
A_2	$\dot{\varepsilon} \leqslant 0.1/\mathrm{s}$	0.2633		
	$\dot{\varepsilon} \geqslant 1.0/\mathrm{s}$	−40.4936		−19.5432
A_3	$\dot{\varepsilon} \leqslant 0.1/\mathrm{s}$	0.07		
	$\dot{\varepsilon} \geqslant 1.0/\mathrm{s}$	16.4124		9.04420

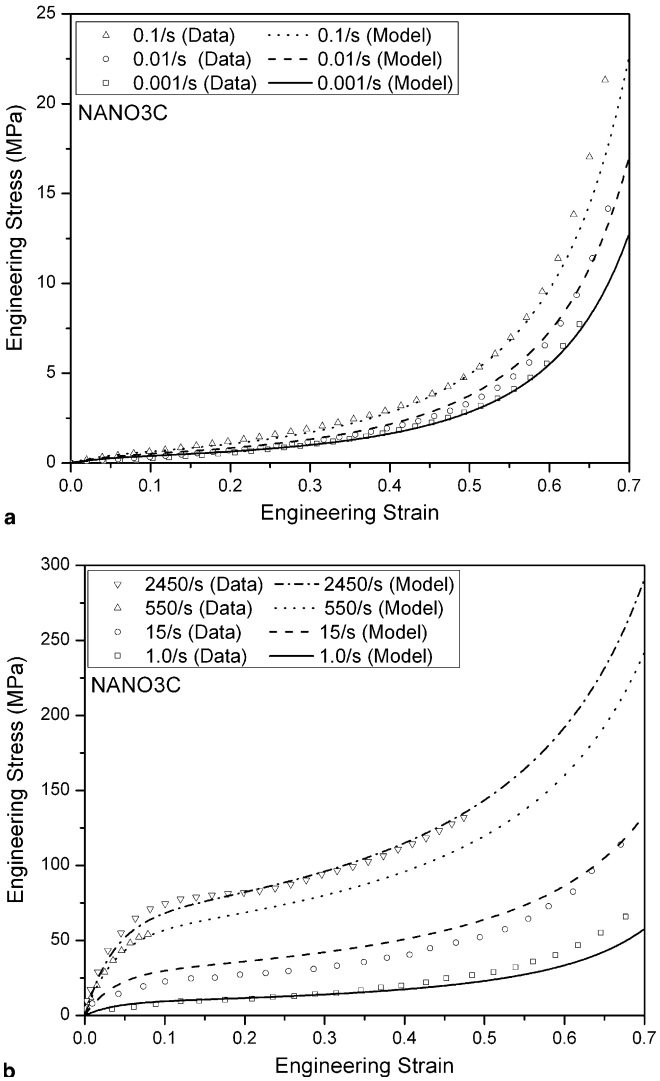

Fig. 10. Comparison of stress–strain curves for ESO/clay-0 at various strain rates by material model and experimental data. (a) $\dot{\varepsilon} \leqslant 0.1/\mathrm{s}$; (b) $\dot{\varepsilon} \geqslant 1.0/\mathrm{s}$.

where A_1, A_2, A_3, and t_1 are material constants; and $\dot{\varepsilon}_0$ is a reference strain-rate. It is noted that the stress (σ_T) and strain (ε) in Eq. (2) are true stress and engineering strain, respectively. Under the assumption of incompressible solids, the true stress in Eq. (2) can be converted into engineering stress (σ_E),

$$\sigma_E = \frac{\sigma_T}{1-\varepsilon} \tag{5}$$

Substitution of Eqs. (3)–(5) into Eq. (2) leads to the material model in engineering stress–strain description,

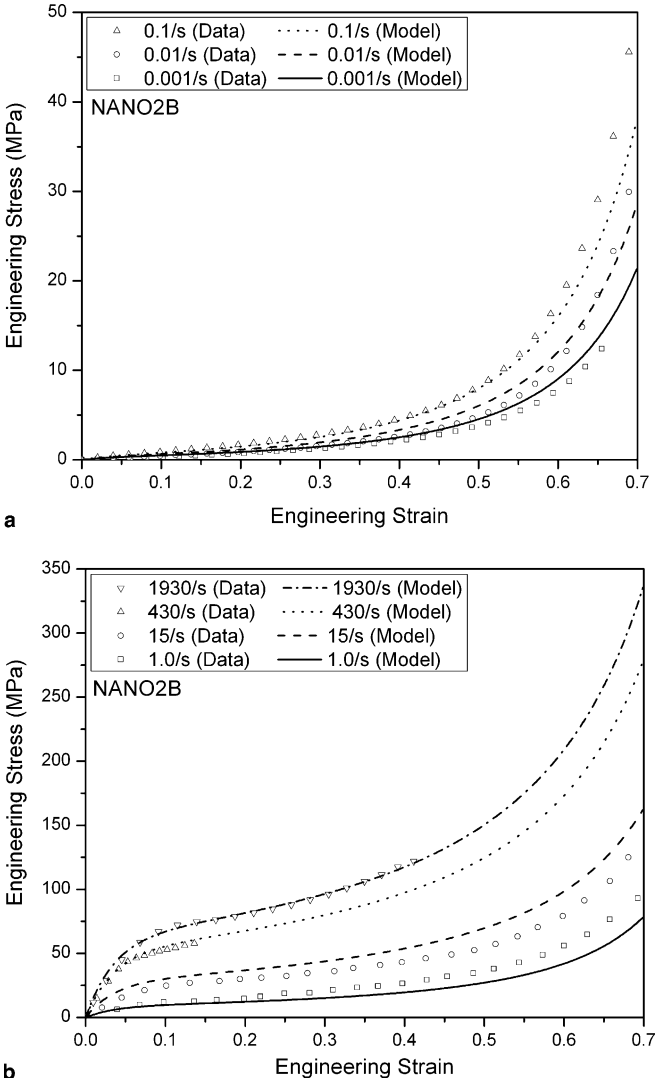

Fig. 11. Comparison of stress–strain curves for ESO/clay-5 at various strain rates by material model and experimental data. (a) $\dot{\varepsilon} \leqslant 0.1/\mathrm{s}$; (b) $\dot{\varepsilon} \geqslant 1.0/\mathrm{s}$.

$$\sigma_{\mathrm{E}} = A_1\left(\frac{\dot{\varepsilon}}{\dot{\varepsilon}_0}\right)^{t_1}\cdot\left(1-\frac{1}{(1-\varepsilon)^3}\right)+\left(\frac{1}{1-\varepsilon}\right)\cdot\left(A_2+A_3\log\frac{\dot{\varepsilon}}{\dot{\varepsilon}_0}\right)\cdot\left(1-\mathrm{e}^{-\frac{\varepsilon}{\varepsilon_r}}\right) \tag{6}$$

The six material constants (or five independent material constants) in Eq. (6) for ESO/clay-0, ESO/clay-5, and ESO/clay-8 were determined by the low strain-rate and high strain-rate experimental results, as tabulated in Table 2. It is observed that varying nanoclay weights produce various strain-rate sensitivities of the nanocomposites. Comparing the material constants for ESO/clay-0 and ESO/clay-5, the values of materials constants are the same except for A_1, indicating that the nanoclay only affects the viscoelastic relaxation

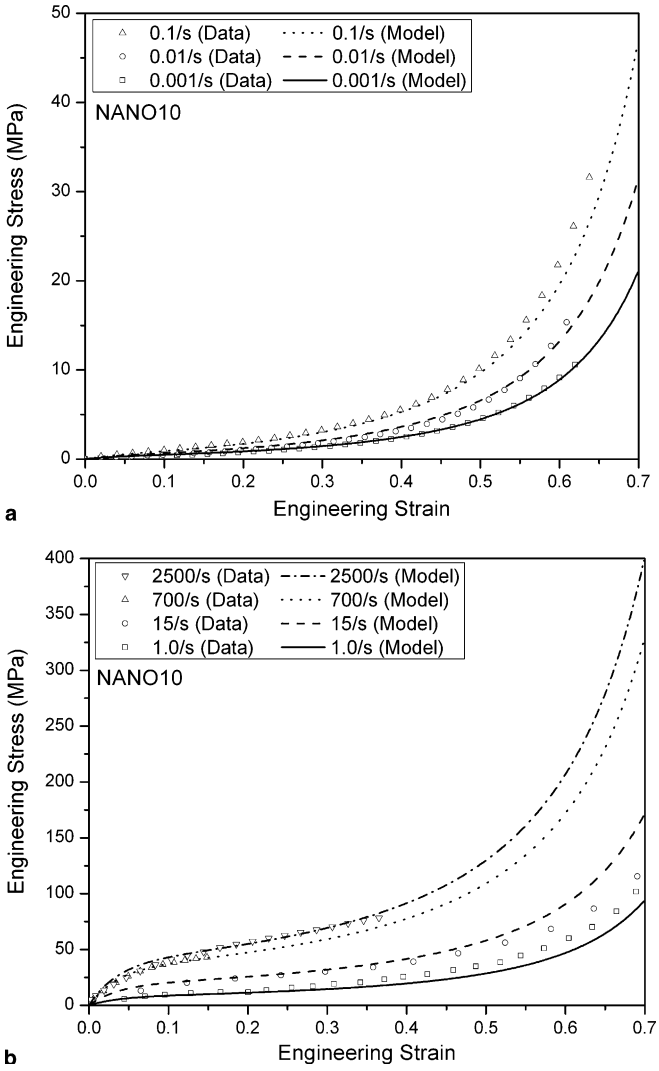

Fig. 12. Comparison of stress–strain curves for ESO/clay-8 at various strain rates by material model and experimental data. (a) $\dot{\varepsilon} \leqslant 0.1/\mathrm{s}$; (b) $\dot{\varepsilon} \geqslant 1.0/\mathrm{s}$.

stress at small strains. At large strains, the nanoclay of 5% weight (ESO/clay-5) improves the compressive properties as compared to the material without nanoclay. When the nanoclay weight increases to 8%, significant effects of nanoclay are observed. At the low strain rates ($\dot{\varepsilon} < 0.1/\mathrm{s}$), the increasing nanoclay weight in materials leads to higher stresses at large strains, but little increase in stress at small strains. At the higher strain rates ($\dot{\varepsilon} \geqslant 1.0/\mathrm{s}$), the material with nanoclay of 8% weight had lower compressive stresses at certain strains than the other materials.

Figs. 10–12 show the comparisons of engineering stress – strain curves at various strain rates from 10^{-3}/s to 10^{3}/s as described by the model, Eq. (6), and the corresponding experimental results for ESO/clay-0, ESO/clay-5, and ESO/clay-8, respectively. It is observed that the one-dimensional stress–strain model accurately describes the compressive behavior of the three nanocomposites at various strain rates. This strain-rate-dependent material model also possesses a form that is relatively simple with a relatively small number of material constants, which makes it feasible to be embedded in numerical simulation codes for the purposes of engineering design and optimization. It is noted that the model accuracy can be further improved through increasing the number of terms in the model, and thus the number of material constants.

4. Conclusions

Quasi-static and dynamic compressive mechanical responses of three ESO/clay materials at various strain rates have been experimentally determined. Nearly constant strain-rate deformation in specimen under dynamic stress equilibrium through pulse-shaping in the high strain-rate experiments yielded valid stress–strain curves at those strain rates. All three nanocomposites exhibited significant strain-rate sensitivities and non-linear behaviors. Strain-rate hardening was observed for all three materials except for the high strain-rate response for the composite with the most nanoclay. The effects of nanoclay on the material strength were found to be mixed. The nanoclay is shown to have positive effects on the nanocomposites only at low strain rates. It has little or negative effects at high strain rates. A one-dimensional material model, combining a strain-rate-dependent strain-energy function and a relaxation function, was used to phenomenologically describe the strain-rate dependent behavior of the three materials at both large and small strains and at both high and low strain rates. This simple material model, with five independent material constants, describes the experimental results well.

References

Abdalla, M.O., Dean, D., Campbell, S., 2002. Viscoelastic and mechanical properties of thermoset PMR-type polyimide–clay nanocomposites. Polymer 43, 5887–5893.

Ahmadi, S.J., Huang, Y.D., Li, W., 2005. Morphology and characterization of clay-reinforced EPDM nanocomposites. J. Comp. Mat. 39, 745–754.

Chen, C., Wang, Y., 1997. An extended nonlinear mechanical model for solid-filled Mooney–Rivlin rubber composites. Polymer 38, 571–576.

Chen, W., Lu, F., Frew, D.J., Forrestal, M.J., 2002. Dynamic compressive testing of soft materials. J. Appl. Mech. – T. ASME 69, 214–223.

Chen, L., Wong, S., Pisharath, S., 2003. Fracture properties of nanoclay-filled polypropylene. J. Appl. Polym. Sci. 88, 3298–3305.

Colak, O.U., 2005. Modeling deformation behavior of polymers with viscoplasticity theory based on overstress. Int. J. Plast. 21, 145–160.

Drozdov, A.D., Christiansen, J.deC., Gupta, R.K., Shah, A.P., 2003. Model for anomalous moisture diffusion through a polymer–clay nanocomposite. J. Polym. Sci. Polym. Phys. 41, 476–492.

Giannelis, E.P., 1996. Polymer layered silicate nanocomposites. Adv. Mater. 8, 29–35.

Ha, Y., Thomas, E.L., 2002. Deformation behavior of a roll-cast layered-silicate/lamellar triblock copolymer nanocomposite. Macromolecules 35, 4419–4428.

Hamley, I.W., 2003. Nanotechnology with soft materials. Angew. Chem. Int. Ed. 42, 1692–1712.

Hao, J., Yuan, M., Deng, X., 2002. Biodegradable and biocompatible nanocomposites of poly(ε-caprolactone) with hydroxyapatite nanocrystals: thermal and mechanical properties. J. Appl. Polym. Sci. 86, 676–683.

Hwu, J.M., Jiang, G.J., Gao, Z.M., Xie, W., Pan, W.P., 2002. The characterization of organic modified clay and clay-filled PMMA nanocompsite. J. Appl. Polym. Sci. 83, 1702–1710.

Khan, A.S., Lopez-Pamies, O., Kazmi, R., 2006. Thermo-mechanical large deformation response and constitutive modeling of viscoelastic polymers over a wide range of strain rates and temperatures. Int. J. Plast. 22, 581–601.

Kim, B.K., Seo, J.W., Jeong, H.M., 2003. Morphology and properties of waterborne polyurethane/clay nanocomposites. Eur. Polym. J. 39, 85–91.

Kinlock, A.J., Taylor, A.C., 2003. Mechanical and fracture properties of epoxy/inorganic micro- and nano-composites. J. Mater. Sci. Lett. 22, 1439–1441.

Kojima, Y., Usuki, A., Kawasumi, M., Okada, A., Kurauchi, T., Kamigaito, O., 1993a. Synthesis of nylon 6–clay hybrid by montmorillonite intercalated with ε-caprolactam. J. Polym. Sci. Polym. Chem. 31, 983–986.

Kojima, Y., Usuki, A., Kawasumi, M., Okada, A., Fukushima, Y., Kurauchi, T., Kamigaito, O., 1993b. Mechanical properties of nylon 6–clay hybrid. J. Mater. Res. 8, 1185–1189.

Kojima, Y., Usuki, A., Kawasumi, M., Okada, A., Kurauchi, T., Kamigaito, O., 1993c. Sorption of water in nylon 6–clay hybrid. J. Appl. Polym. Sci. 49, 1259–1264.

Kojima, Y., Usuki, A., Kawasumi, M., Okada, A., Kurauchi, T., Kamigaito, O., 1993d. One-pot synthesis of nylon 6–clay hybrid. J. Polym. Sci. Polym. Chem. 31, 1755–1758.

Kojima, Y., Fukumori, K., Usuki, A., Okada, A., Kurauchi, T., 1993e. Gas permeabilities in rubber–clay hybrid. J. Mater. Sci. Lett. 12, 889–890.

Kojima, Y., Usuki, A., Kawasumi, M., Okada, A., Kurauchi, T., Kamigaito, O., Kaji, K., 1994. Fine structure of nylon-6–clay hybrid. J. Polym. Sci. Polym. Phys. 32, 625–630.

Kojima, Y., Usuki, A., Kawasumi, M., Okada, A., Kurauchi, T., Kamigaito, O., Kaji, K., 1995. Novel preferred orientation in injection-molded nylon 6–clay hybrid. J. Polym. Sci. Polym. Phys. 33, 1039–1045.

Kolsky, H., 1949. An investigation of mechanical properties of materials at very high rates of loading. Proc. Phys. Soc. Lond. B62, 676–700.

Kornmann, X., Thomann, R., Mülhaupt, R., Finter, J., Berglung, L., 2002. Synthesis of amine-cured, epoxy-layered silicate nanocomposites: the influence of silicate surface modifications on the properties. J. Appl. Polym Sci. 86, 2643–2652.

Lan, T., Pinnavaia, T.J., 1994. Clay-reinforced epoxy nanocomposites. Chem. Mater. 6, 2216–2219.

LeBaron, P.C., Wang, Z., Pinnavaia, T.J., 1999. Polymer-layered silicate nanocomposites: an overview. Appl. Clay Sci. 15, 11–29.

Lee, J.H., Park, T.G., Park, H.S., Lee, D.S., Lee, Y.K., Yoon, S.C., Nam, J.D., 2003. Thermal and mechanical characteristics of poly(L-lactic acid) nanocomposite scaffold. Biomaterials 24, 2773–2778.

Lion, A., Kardelky, C., 2004. The Payne effect in finite viscoelasticity constitutive modelling based on fractional derivatives and intrinsic time scales. Int. J. Plast. 20, 1313–1345.

Liu, T., Lim, K.P., Tjiu, W.C., Pramoda, K.P., Chen, Z.K., 2003. Preparation and characterization of nylon 11/organoclay nanocomposites. Polymer 44, 3529–3535.

Makradi, A., Ahzi, S., Gregory, R.V., Edie, D.D., 2005. A two-phase self-consistent model for the deformation and phase transformation behavior of polymers above the glass transition temperature: application to PET. Int. J. Plast. 21, 741–758.

Nam, P.H., Maiti, P., Okamoto, M., Kotaka, T., Hasegawa, N., Usuki, A., 2001. A hierarchical structure and properties of intercalated polypropylene/clay nanocomposites. Polymer 42, 9633–9640.

Ogden, R.W., Roxburgh, D.G., 1999. An energy-based model for the Mullins effect. In: Dorfmann, A., Muhr, A. (Eds.), Constitutive Models for Rubber. Taylor & Francis Ltd, London, pp. 23–28.

Okada, A., Usuki, A., 1995. The chemistry of polymer–clay hybrids. Mat. Sci. Eng. C-Bio. S. 3, 109–115.

Okada, A., Kawasumi, M., Usuki, A., 1989. Nylon 6-Clay hybrid. In: Schaefer, D.W., Mark, J.E. (Eds.), Polymer Based Molecular Composites. Materials Research Society Symposium Proceedings, vol. 171, Boston, MA, pp. 45–50.

Ravichandran, G., Subhash, G., 1994. Critical appraisal of limiting strain rates for compression testing of ceramics in a split Hopkinson pressure bar. J. Am. Ceram. Soc. 77, 263–267.

Song, B., Chen, W., 2004. Dynamic stress equilibrium in split Hopkinson pressure bar tests on soft materials. Exp. Mech. 44, 300–312.

Song, B., Chen, W., Cheng, M., 2004. Novel model for uniaxial strain-rate-dependent stress–strain behavior of ethylene-propylene-diene monomer rubber in compression or tension. J. Appl. Polym. Sci. 92, 1553–1558.

Sur, G.S., Sun, H.L., Lyu, S.G., Mark, J.E., 2001. Synthesis, structure, mechanical properties, and thermal stability of some polysulfone/organoclay nanocomposites. Polymer 42, 9783–9789.

Svoboda, P., Zeng, C., Wang, H., Lee, L.J., Tomasko, D.L., 2002. Morphology and mechanical properties of polypropylene/organoclay nanocomposite. J. Appl. Polym. Sci. 85, 1562–1570.

Tien, Y.I., Wei, K.H., 2001. High-tensile-property layered silicates/polyurethane nanocomposites by using reactive silicates as pseudo chain extenders. Macromolecules 34, 9045–9052.

Tyan, H., Wei, K., Hsieh, T., 2000. Mechanical properties of clay–polyimide (BTDA-ODA) nanocomposites via ODA-modified organoclay. J. Polym. Sci. Polym. Phys. 38, 2873–2878.

Uribe-Arocha, P., Mehler, C., Puskas, J.E., Altstädt, V., 2003. Effect of sample thickness on the mechanical properties of injection-molded polyamide-6 and polyamide-6 clay nanocomposites. Polymer 44, 2441–2446.

Usuki, A., Koiwai, A., Kojima, Y., Kawasumi, M., Okada, A., Kurauchi, T., Kamigaito, O., 1995. Interaction of nylon 6–clay surface and mechanical properties of nylon 6–clay hybrid. J. Appl. Polym. Sci. 55, 119–123.

Wang, L.L., Huang, D., Gan, S., 1995. Nonlinear viscoelastic constitutive relations and nonlinear viscoelastic wave propagation for polymers at high strain rates. In: Kawata, K., Shioiri, J. (Eds.), Constitutive Relations in High/very High Strain Rates, IUTAM Symposium, Noda, Japan, pp. 137–146.

Wanjale, S.D., Jog, J.P., 2003. Effect of modified layered silicates and compatibilizer on properties of PMP/clay nanocomposites. J. Appl. Polym. Sci. 90, 3233–3238.

Ward, I.M., 1983. Mechanical Properties of Solid Polymers, second ed. Wiley, New York.

Young, S.K., Mauritz, K.A., 2002. Nafion®/(organically modified silicate) nanocomposites via polymer in situ sol–gel reactions: mechanical tensile properties. J. Polym. Sci. Polym. Phys. 40, 2237–2247.

Zerda, A.S., Lesser, A.J., 2001. Intercalated clay nanocomposites: morphology, mechanics, and fracture behavior. J. Polym. Sci. Polym. Phys. 39, 1137–1146.

Zhang, G., Shichi, T., Takagi, K., 2003. PET–clay hybrids with improved tensile strength. Mater. Lett. 57, 1858–1862.

Zhou, W., Mark, J.E., Unroe, M.R., Arnold, F.E., 2001. Some clay nanocomposites based on a high-temperature, high performance polymer. J. Macromol. Sci. Pure A38, 1–9.